Numerical Solution of the Beam Equation for Beams subject to Large Deflections

Magnus Komperød[1]

[1]Technological Analyses Centre, Nexans Norway AS, Norway, magnus.komperod@nexans.com

Abstract

The bending stiffness of subsea cables and umbilicals can be identified from physical tests where the cable is supported at both ends and then pushed or pulled at the center. The beam equation can be used to calculate the bending stiffness from the measured force and the measured deflection. However, a study performed by Nexans Norway AS shows that the beam equation oversimplifies the cables' properties and thereby disregards significant effects. This paper extends the beam equation into the case of large deflections, which is the second milestone of the work on deriving an accurate model. Within a realistic range of cable deflections, the force calculated by the novel model differs with up to 20% compared to the previous, oversimplified model. From the author's point of view, this large difference justifies the somewhat increased complexity and computation time of the novel model.

Keywords: Beam Equation, Bending Stiffness, Large Deflection, Minimum Total Potential Energy Principle, Numerical Analysis, Subsea Power Cable, Umbilical.

1 Introduction

Mathematical models and finite element analyses of subsea power cables' and umbilicals' mechanical properties are used to calculate the mechanical stresses that arise when the cable is subject to external loads such as axial tension, bending, and twisting. Mathematical models of cables have been presented in the scientific literature at least since the 1960s; for example Lutchansky (1969) which is still relevant today. The field has matured since then by improving the models and including additional effects. Among the most comprehensive publications on models of cables' mechanical properties is the excellent PhD thesis of Kebadze (2000).

Physical testing of cables are necessary to validate the mathematical models and the finite element analyses. However, the test rigs themselves inherently introduce new, often complex, properties to the overall system, which make it difficult to separate the cable properties from the rig properties in the measurement data. Further, the rig sensors do not measure the desired cable properties directly. Hence, mathematical models have to be developed for calculating the desired cable properties based the sensor signals. For some kinds of physical cable tests, including bending stiffness tests, developing such models are complex and challenging tasks.

Unfortunately, the scientific literature is sparse on physical tests of cables, and in particular sparse on models for calculating the desired cable properties from the sensor signals. Maioli (2015) presents results on traditional deflection tests as sketched in Figure 1. This publication uses beam theory derived for small deflections to calculate the cables' bending stiffness, despite the actual deflections may be rather large. Tarnowski (2015) presents results from a similar test, but with a bending stiffness calculation model that intends to handle large deflections. Also Ekeberg and Dhaigude (2016) and Dhaigude and Ekeberg (2016) present bending tests. However, these papers are sparse on the details of the calculation model.

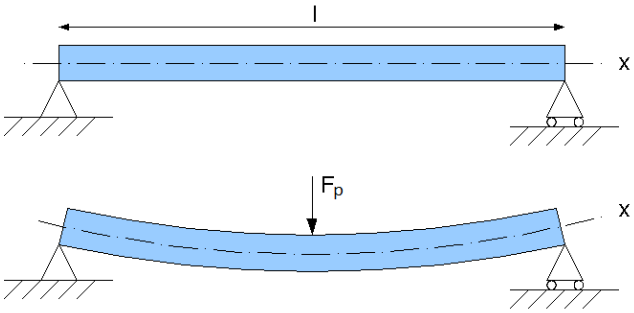

Figure 1. Sketch of bending stiffness rig. Illustration from www.wikimedia.org.

Nexans Norway AS is currently performing several R&D activities on improving modeling and physical testing of subsea power cables' and umbilicals' mechanical properties. As part of this work a novel bending stiffness rig has been developed. The rig is based on the principle sketched in Figure 1 and its details are presented in Jordal et al. (2017). Initially the cables' bending stiffness was calculated from the rig's sensors as presented in Komperød et al. (2017), which is essentially the beam equation derived for small deflections, followed by filtering and postprocessing to improve the signal quality. However, a more detailed study of cables' behavior under bending revealed that this approach is an oversimplification. Nexans Norway AS has therefore started an R&D work which aims to correctly model the cable under bending stiffness tests.

The R&D work is split into milestones for easier han-

dling the complexity of the overall modeling problem. Komperød (2018) presents the first milestone which is to rewrite the beam equation using the minimum total potential energy principle and solve this equation numerically. The motivation behind the paper is that the minimum total potential energy principle is believed to be more suitable for extending the beam equation than the force- and moment balances which are commonly used in the scientific literature for deriving this equation. Also, the paper solves the beam equation numerically because it is assumed to be impossible to solve the extended beam equation analytically.

The present paper derives and presents the results of the second milestone, which is to consistently handle large deflections. This is an important step towards correctly modeling the cables' bending stiffness based on the sensors of the bending stiffness rig, because the physical tests are often performed with large deflections. The improvement of the novel model will be demonstrated by comparing it to the model of Komperød (2018).

2 Nomenclature

Table 1 presents the main nomenclature used in this paper. Variables without an intuitive physical meaning are defined in the main text where they first appear.

Table 1. Nomenclature.

$\bar{\mathbf{c}}$	Vector with Clenshaw-Curtis quadrature weights.
$\mathbf{D}_1$	Chebyshev first-derivative matrix.
$\mathbf{D}_2$	Chebyshev second-derivative matrix.
EI	Bending stiffness [Nm/(m^{-1})].
F_p	Deflection force [N].
g	Acceleration of gravity [m/s^2].
L	Length between supports [m].
M	Bending moment [Nm].
$\tilde{m}$	Mass per unit length [kg/m].
N	Number of discretization points [-].
$\bar{N}$	Number of discretization points over a half beam [-].
P	Total potential energy [J].
P_g	Gravitational energy [J].
P_s	Strain energy [J].
s	Beam length parameter [m].
u	Vertical deflection of beam [m].
u_p	Vertical deflection of piston [m].
$\mathbf{u}$	Vector containing discrete points of u.
x	Coordinate along x-axis [m].
κ	Bending curvature [m^{-1}].
λ_i	Lagrange multiplier no. i.

Vectors are denoted with lower case, bold font. Matrices are denoted with upper case, bold font. Square bracket are used to denote parts of a vector or a matrix. For example $\mathbf{A}[1:4,3]$ means the first four rows of the third column of $\mathbf{A}$.

The symbol $\bullet$ means vector dot product. The symbol $\cdot$ applied to vectors and matrices, for example $\mathbf{a}\cdot\mathbf{b}$, means element-by-element multiplication. Exponent notation applied to a vector, for example $\mathbf{x}^2$, means element-by-element exponent.

Figure 2 shows the Cartesian coordinate system used in this paper.

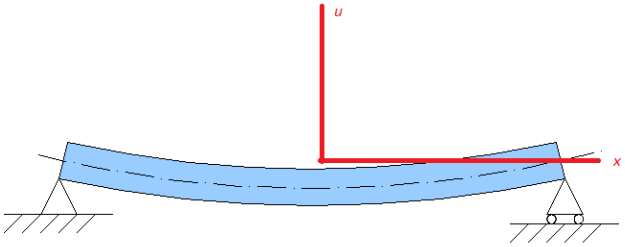

Figure 2. The Cartesian coordinate system used in this paper. Based on illustration from www.wikimedia.org.

3 Assumptions and Simplifications

The mathematical derivation in this paper is subject to the following assumptions and simplifications:

1. The beam is made of a linear, elastic material and has identical cross section over its entire length.
2. Only the beam segment between the supports shown in Figure 1 is considered. That is, possible beam segments outside these supports are disregarded.
3. The beam is assumed not to move horizontally at the center of its length, i.e. where the F arrow points in Figure 1. During the physical bending stiffness tests this constraint is enforced by the design of the bending stiffness rig.
4. The developed model is quasi-static, i.e. inertia and kinetic energy are disregarded.
5. The height of the beam is small compared to the length between the beam supports, L.

4 Total Potential Energy and Constraints

In Komperød (2018) the total potential energy, P, was found to be

$$P = \frac{1}{2}\mathrm{EI} \int_{\text{beam length}} \kappa^2 \, \mathrm{d}s \tag{1}$$

$$+ \tilde{m} g \int_{\text{beam length}} u \, \mathrm{d}s.$$

The upper right term of Eq. 1 is the beam's strain energy due to bending, while the lower right term is the beam's gravitational energy. In the equation EI is the beam's bending stiffness and κ is its bending curvature, while s is the cable length parameter. Further, $\tilde{m}$ and g are the beam's mass per unit length and the acceleration of gravity, respectively, and u is the beam's deflection. u is a function of s, while κ is a function of the first- and second derivatives of u.

Also the constraints were found in Komperød (2018). They are

$$u(\text{left end}) = 0, \tag{2}$$

$$u(\text{center}) = u_\mathrm{p}, \tag{3}$$

$$u(\text{right end}) = 0, \tag{4}$$

$$u(s) \in C^2. \tag{5}$$

The constraints of Eqs. 2, 3, and 4 follow directly from the rig design as sketched in Figure 1. In Eq. 3, u_p is the position of the piston which applies the force F_p.

In Eq. 5, C^2 is the set all functions which are continuous and have continuous first- and second derivatives (and possibly continuous higher order derivatives). Hence, the practical interpretation of this constraint is that the beam's deflection, deflection angle, and curvature are continuous. The third derivative is known to be discontinuous at the point load F_p of Figure 1. These results are all well known from beam theory.

5 Numerical Solution

The overall problem is to minimize the total potential energy, i.e. Eq. 1, w.r.t. the constraints given by Eqs. 2 - 5. This section solves this problem using numerical mathematics.

5.1 Calculating the Total Potential Energy

The total potential energy is given by Eq. 1. In order to be calculated numerically, the integration limits must be expressed numerically, and the curvature κ must be expressed in terms of the deflection u.

It is more convenient to use the horizontal coordinate x, rather than the cable length parameter s, as the integration variable. The arc length formula relates x and s, i.e.

$$\mathrm{d}s = \left[1 + \left(\frac{\mathrm{d}u}{\mathrm{d}x}\right)^2\right]^{\frac{1}{2}} \mathrm{d}x. \tag{6}$$

Using x as the integration variable and the Cartesian coordinate system of Figure 2 gives that the integration limits are $-\frac{L}{2}$ and $\frac{L}{2}$, where L is the distance between the beam supports. The curvature is related to the deflection by

$$\kappa = \frac{\mathrm{d}^2 u}{\mathrm{d}x^2}\left[1 + \left(\frac{\mathrm{d}u}{\mathrm{d}x}\right)^2\right]^{-\frac{3}{2}}. \tag{7}$$

Hence, Eq. 1 can be written as

$$P = \frac{1}{2}\mathrm{EI} \int_{-L/2}^{L/2} \left(\frac{\mathrm{d}^2 u}{\mathrm{d}x^2}\right)^2 \left[1 + \left(\frac{\mathrm{d}u}{\mathrm{d}x}\right)^2\right]^{-\frac{5}{2}} \mathrm{d}x \tag{8}$$

$$+ \tilde{m} g \int_{-L/2}^{L/2} u \left[1 + \left(\frac{\mathrm{d}u}{\mathrm{d}x}\right)^2\right]^{\frac{1}{2}} \mathrm{d}x.$$

Similar to in Komperød (2018), the unknown u that minimizes the total potential energy can not be calculated directly. Instead u will be calculated at discrete, Chebyshev-distributed points which can later be interpolated. The points will be Chebyshev-distributed over the left half of the beam, and Chebyshev-distributed over the right half of the beam, rather than being Chebyshev-distributed over the entire beam. This is done to avoid that the discontinuity of the third derivative at the center point disturbs the excellent convergence properties of Chebyshev series for functions in C^∞.

Let $\mathbf{u}$ be a vector with the N discrete points of u, where N is an even number. It is convenient to introduce

$$\bar{N} = N/2, \tag{9}$$

$$\bar{\mathbf{u}}_\mathrm{L} = \mathbf{u}[1 : \bar{N}], \tag{10}$$

$$\bar{\mathbf{u}}_\mathrm{R} = \mathbf{u}[\bar{N} + 1 : N]. \tag{11}$$

Hence, $\bar{\mathbf{u}}_\mathrm{L}$ is the discrete points of u on the left half of the beam, and $\bar{\mathbf{u}}_\mathrm{R}$ is the discrete points of the right half. Note that the last element of $\bar{\mathbf{u}}_\mathrm{L}$ must be equal to the first element of $\bar{\mathbf{u}}_\mathrm{R}$, because they both equals the piston deflection, u_p. This will later be enforce through a constraint.

The first and second derivative of u at the Chebyshev nodes can be calculated using the Chebyshev first-derivative and second-derivative matrices $\mathbf{D}_1$ and $\mathbf{D}_2$. Once the total potential energy per unit length is calculated at the Chebyshev nodes, the total potential energy

over the beam can be calculated using Clenshaw-Curtis quadrature. Both the Chebyshev derivative matrices and Clenshaw-Curtis quadrature are explained in Reid (2014). Hence, the total potential energy over the beam is

$$P = \frac{\mathrm{EI}L}{8}\left((\mathbf{D}_2\bar{\mathbf{u}}_\mathrm{L})^2 \cdot \left[\mathbf{1}_{\bar{N}\times 1} + (\mathbf{D}_1\bar{\mathbf{u}}_\mathrm{L})^2\right]^{-\frac{5}{2}}\right) \bullet \bar{\mathbf{c}} \quad (12)$$

$$+ \frac{\mathrm{EI}L}{8}\left((\mathbf{D}_2\bar{\mathbf{u}}_\mathrm{R})^2 \cdot \left[\mathbf{1}_{\bar{N}\times 1} + (\mathbf{D}_1\bar{\mathbf{u}}_\mathrm{R})^2\right]^{-\frac{5}{2}}\right) \bullet \bar{\mathbf{c}}$$

$$+ \frac{\tilde{m}gL}{4}\left(\bar{\mathbf{u}}_\mathrm{L} \cdot \left[\mathbf{1}_{\bar{N}\times 1} + (\mathbf{D}_1\bar{\mathbf{u}}_\mathrm{L})^2\right]^{\frac{1}{2}}\right) \bullet \bar{\mathbf{c}}$$

$$+ \frac{\tilde{m}gL}{4}\left(\bar{\mathbf{u}}_\mathrm{R} \cdot \left[\mathbf{1}_{\bar{N}\times 1} + (\mathbf{D}_1\bar{\mathbf{u}}_\mathrm{R})^2\right]^{\frac{1}{2}}\right) \bullet \bar{\mathbf{c}}.$$

In Eq. 12 all vectors are of dimension $\bar{N}\times 1$ and all matrices are of dimension $\bar{N}\times\bar{N}$. The vector $\bar{\mathbf{c}}$ is the vector of the Clenshaw-Curtis quadrature weights for the standard integration interval $[-1\,,\,1]$. The vector $\mathbf{1}$ is the vector which all elements are 1 and its dimension is given by the subscript. On the right side of Eq. 12 the first row is the strain energy of the left half of the beam, the second row is the strain energy of the right half of the beam, the third row is the gravitational energy of the left half of the beam, and the forth row is the gravitational energy of the right half of the beam.

5.2 Constraints

The overall problem to be solved is to minimize Eq. 12 subject to the constraints of Eqs. 2 - 5. This section considers how to implement these constraints, while the subsequent sections present how to solve the optimization problem.

The constraints of Eq. 2 and Eq. 4 are straight forward to implement; they become

$$\mathbf{u}[0] = 0, \quad (13)$$

$$\mathbf{u}[N] = 0. \quad (14)$$

Because two vector elements of $\mathbf{u}$ represent the deflection at center, i.e. at $x = 0$, the constraint of Eq. 3 can be implemented in three different ways: (i) $\mathbf{u}[\bar{N}] = u_\mathrm{p}$ and $\mathbf{u}[\bar{N}+1] = u_\mathrm{p}$, (ii) $\mathbf{u}[\bar{N}] = u_\mathrm{p}$ and $\mathbf{u}[\bar{N}+1] = \mathbf{u}[\bar{N}]$, or (iii) $\mathbf{u}[\bar{N}] = \mathbf{u}[\bar{N}+1]$ and $\mathbf{u}[\bar{N}+1] = u_\mathrm{p}$. All choices give the same information, and hence the same results. However, the latter two choices give more straight forward interpretation of the Lagrange multipliers. The second choice is used in this paper. The constraints are then

$$\mathbf{u}[\bar{N}] = u_\mathrm{p}, \quad (15)$$

$$\mathbf{u}[\bar{N}] - \mathbf{u}[\bar{N}+1] = 0. \quad (16)$$

As explained in Komperød (2018), the constraint of Eq. 5 will be obeyed if and only if u and its first- and second derivatives are continuous at $x = 0$. u is continuous by Eq. 16. The first- and second derivatives are continuous by enforcing

$$\mathbf{D}_1[\bar{N},:]\bar{\mathbf{u}}_\mathrm{L} - \mathbf{D}_1[1,:]\bar{\mathbf{u}}_\mathrm{R} = 0, \quad (17)$$

$$\mathbf{D}_2[\bar{N},:]\bar{\mathbf{u}}_\mathrm{L} - \mathbf{D}_2[1,:]\bar{\mathbf{u}}_\mathrm{R} = 0. \quad (18)$$

The constraints are implemented in the order Eq. 13, Eq. 15, Eq. 16, Eq. 14, Eq. 17, and Eq. 18. Although the total potential energy, i.e. Eq. 12, is nonlinear, all constraints are linear. Hence, the constraints can be written in matrix form as

$$\mathbf{A}\mathbf{u} = u_\mathrm{p}\mathbf{b}, \quad (19)$$

$$\mathbf{A} = \begin{bmatrix} \mathbf{i}_1{}^\mathrm{T} \\ \mathbf{i}_{\bar{N}}{}^\mathrm{T} \\ (\mathbf{i}_{\bar{N}} - \mathbf{i}_{\bar{N}+1})^\mathrm{T} \\ \mathbf{i}_N{}^\mathrm{T} \\ \mathbf{D}_1[\bar{N},:]\,,\, -\mathbf{D}_1[1,:] \\ \mathbf{D}_2[\bar{N},:]\,,\, -\mathbf{D}_2[1,:] \end{bmatrix} \in \mathbb{R}^{6\times N}, \quad (20)$$

$$\mathbf{b} = \begin{bmatrix} 0 \\ 1 \\ 0 \\ 0 \\ 0 \\ 0 \end{bmatrix} \in \mathbb{R}^{6\times 1}. \quad (21)$$

In Eq. 20, $\mathbf{i}_j$ is the jth column of the $N\times N$ identify matrix. Note that in the third row of the matrix $\mathbf{A}$ two vectors of dimension N are subtracted, while in the fifth and sixth rows two vectors of dimension $\bar{N}$ are concatenated into one vector of dimension N.

5.3 Transforming to an Unconstrained Optimization Problem

The vector $\mathbf{u}^*$ that minimizes the constrained optimization problem of Eq. 12 and Eq. 19 must obey Eq. 19. The matrix $\mathbf{A}$ of Eq. 20 has full rank, i.e. rank 6, otherwise the constraints would have been redundant or contradictory. Hence, $\mathbf{A}$ has a nullspace of dimension $N-6$. That is, there are $N-6$ independent vectors that solves the homogeneous equation

$$\mathbf{A}\mathbf{u} = \mathbf{0}_{6\times 1}, \quad (22)$$

where $\mathbf{0}$ is the vector which all elements are zero and its dimension is given by the subscript.

Let $\mathbf{U} \in \mathbb{R}^{N\times(N-6)}$ be a matrix which columns are an orthonormal basis of the nullspace of $\mathbf{A}$. Then the homogeneous equation can be written

$$\mathbf{AUw} = \mathbf{0}_{6\times 1}, \tag{23}$$

where $\mathbf{w} \in \mathbb{R}^{(N-6)\times 1}$ is an arbitrary vector. Further, let $\mathbf{u}_\mathrm{s}$ be a particular solution of the equation

$$\mathbf{Au} = \mathbf{b}. \tag{24}$$

Then, multiplying Eq. 24 by u_p and adding Eq. 23 gives

$$\mathbf{A}\left(u_\mathrm{p}\mathbf{u}_\mathrm{s} + \mathbf{Uw}\right) = u_\mathrm{p}\mathbf{b}. \tag{25}$$

Hence, the deflection vector $\mathbf{u}$ given by

$$\mathbf{u} = u_\mathrm{p}\mathbf{u}_\mathrm{s} + \mathbf{Uw} \tag{26}$$

obeys all constraints for any $\mathbf{w}$. In order words, the $N-6$ elements of $\mathbf{w}$ are the $N-6$ degrees of freedom for minimizing the total potential energy, P, given by Eq. 12. Expressed mathematically, the constrained optimization problem is transformed into the unconstrained optimization problem

$$\mathbf{w}^* = \arg\min_{\mathbf{w}} P(\mathbf{u}(\mathbf{w})). \tag{27}$$

5.4 Initial Values for Iterative Optimization

Because $\mathbf{Uw}$, for any $\mathbf{w}$, added to a particular solution $\mathbf{u}_\mathrm{s}$ gives a new particular solution, there are infinite number of particular solutions that satisfy Eq. 24. An intuitive approach is to calculate a particular solution from Eq. 24 using linear algebra. However, many optimization methods, including Newton's method and Quasi-Newton methods, depend on sufficiently good initial values in order to converge to the global minimum. A solution of Eq. 24 found from linear algebra may be a very poor initial value for the optimization method.

A better method for finding a particular solution that is also a good initial value for the optimization method is to use the analytical solution of the beam equation. Although the analytical solution is valid only for infinitesimal deflections, it is still a decent initial value. For most real-life bending stiffness tests of cables the effect of gravity is small. Hence, the gravity term can be excluded from the analytical solution when calculating the initial values. The analytical solution then becomes

$$u = \begin{cases} -\frac{4}{L^3}x^3 - \frac{6}{L^2}x^2 + 1 & , \quad x < 0 \\ \frac{4}{L^3}x^3 - \frac{6}{L^2}x^2 + 1 & , \quad x \geq 0 \end{cases}. \tag{28}$$

It is trivial to verify that Eq. 28 obeys the constraints of Eqs. 2 - 5 for $u_\mathrm{p} = 1$. Hence, the discrete-point deflection vector $\mathbf{u}$ calculated by evaluating Eq. 28 at the Chebyshev points is a particular solution of Eq. 24 and a good initial value for the optimization method.

A most favorable property of Eq. 28 is that it does not depend on the deflection force, F, or the beam's bending stiffness, EI. This is because the force and the bending stiffness cancel in the calculation of the deflection, u. Actually, calculation of the deflection depends only on the length between the beam supports, L, which is trivial to measure prior to the bending stiffness tests.

If gravity is to be taken into consideration, the particular solution will be somewhat more complex and it will depend on the beam's specific weight, $\tilde{m}$, and its bending stiffness, EI. In other words, an initial guess of the bending stiffness will then be necessary. Please note that even if gravity is neglected when calculating the particular solution, gravity will still be included during the optimization, and hence be included in the final calculation of the deflection.

5.5 Iterative Optimization

The approach presented in Section 5.4 provides good initial values, which significantly ease the iterative optimization process. The results presented in this paper will in future work be extended with (i) nonlinear materials and (ii) shear forces of helical cable elements. Because these extensions may significantly change the characteristics of the optimization problem, the choice of optimization method has not yet been settled.

Also the choice of number of nodes, N, will need further attention. Too few nodes will not provide sufficient flexibility to represent the beam's or cable's true behavior. However, a large number of nodes increase the computation time and may increase the risk that the optimization algorithm get trapped in a local minimum or fails due to accumulations of arithmetic errors.

The *preliminary* conclusions based on the work done so far are:

1. Good choices of N seems to be in the range 14 to 20, i.e. $\bar{N}$ in the range 7 to 10. Higher values of N give no or insignificant reduction of the total potential energy, P. Lower values of N gives somewhat increased P, which indicates insufficient flexibility to resemble the beam's true deflection profile. The proposed range of N gives rapid convergence and no issues with local minima or arithmetic errors have been observed.

2. Newton's method converges very rapidly and no failures have been observed in the proposed range of N. The method converges also for $N = 50$, while it fails for $N = 100$. The intermediate values have not been tested. Calculation of the elements of the Hessian matrix and the gradient vector are done numerically using finite differences, because analytical calculations will not be an option after implementing non-

linear materials and shear forces. After implementing these improvements, calculation of the Hessian matrix may be expensive in terms of CPU load.

3. The gradient decent method performs poorly; it converges very slowly for small values of N, and it fails to reach the global minimum for larger N.

4. The Broyden–Fletcher–Goldfarb–Shanno (BFGS) method can roughly be considered a hybrid between the gradient decent method and Newton's method; it starts off identically to the gradient decent method and then uses the information gained during the iterations to build an estimate of the Hessian matrix, which makes it gradually resemble the properties of Newton's method.

   Similar to Newton's method, the BFGS method performs very well within the proposed range of N. Actually, the BFGS method converges to the global minimum for $N = 100$, where the two former methods both fail. The BFGS method fails for $N = 200$, while the intermediate values have not been tested.

   The BFGS method avoids the expensive computation of the Hessian matrix. However, the method requires a larger number of iterations than Newton's method, and may require several calculations of the total potential energy, P, to get the correct step length within each iteration. Hence, further study must be performed in order to conclude whether Newton's method or the BFGS method is the most efficient for this particular optimization problem.

6 Calculating Deflection Force

In the physical bending stiffness rig the piston's deflection, u_p, and deflection force, F_p, are measured. Hence, comparisons between the physical tests and the cable model will focus on these variables. In the model the deflection is given as a constraint, while the force is to be calculated. The force is given as the derivative of the total potential energy w.r.t. the deflection, i.e.

$$F_\mathrm{p} = \frac{\partial P}{\partial u_\mathrm{p}}. \tag{29}$$

Based on Eq. 29 the force can be calculated using finite differences or the Chebyshev first-derivative matrix $\mathbf{D}_1$.

The motivation behind the work presented in this paper is to improve the calculations derived in Komperød (2018), because the latter depend on simplifications which are valid only for infinitesimal deflections. It is then of interest to compare the two calculation methods to answer whether they differ significantly or not. Figure 3 presents the calculated deflection force, F_p, as function of the deflection, u_p, for the two approaches. The calculations are done for a steel tube with bending stiffness 124.1 kNm^2 and specific mass 8.257 kg/m. The distance between the supports are 3.000 m. The interval $u_\mathrm{p} \in [-0.4\,,\,0.4]$ is the range of the piston on the bending stiffness rig. The BFGS method with $N = 20$ was used.

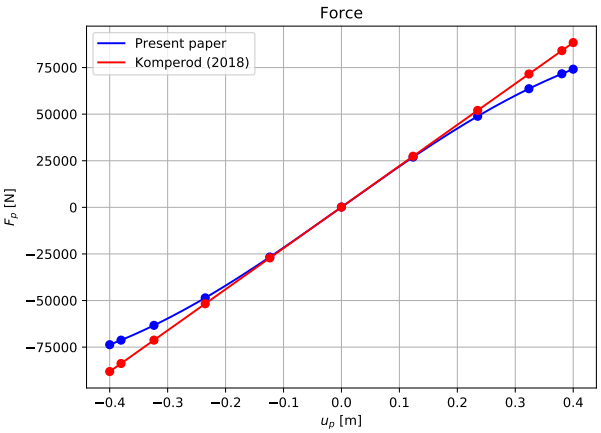

Figure 3. Deflection force calculated from the present paper and from Komperød (2018). The dots represent Chebyshev-distributed points and the lines represent interpolations between these points. For the present paper the force is calculated using Eq. 29 and the Chebyshev first-derivative matrix $\mathbf{D}_1$. For Komperød (2018) the force is calculated from Lagrange multipliers as explained in that paper.

As seen from Figure 3, the two approaches give near identical results for small deflections, i.e. deflections close to zero, while the model of Komperød (2018) becomes increasingly inaccurate for larger deflections. Figure 4 shows the relative error of Komperød (2018) compared to the calculations derived in the present paper. As seen from the figure, the relative error resembles a parabola quite well. Hence, the relative error increases approximately by the deflection squared. The reason behind this relationship has not been studied. The largest relative error shown in the figure is almost 20%.

Based on Figures 3 and 4, it is concluded that the approach of Komperød (2018) gives high accuracy for small deflections, but should be avoided for larger deflections. This result was expected because Komperød (2018) is based on the assumption of infinitesimal deflections. Please note that the deflection range for which the latter approach will give high accuracy will depend on the length between the supports, L. Therefore, the error indicated by Figures 3 and 4 should not be generalized to arbitrary values of L.

7 On Lagrange Multipliers

In the present paper, the author chooses to use the constraints to reduce the number of variables and hence improve the convergence of the optimization problem. In Komperød (2018) the constraints are handled using Lagrange multipliers, which give additional information as the majority of the Lagrange multipliers have physical in-

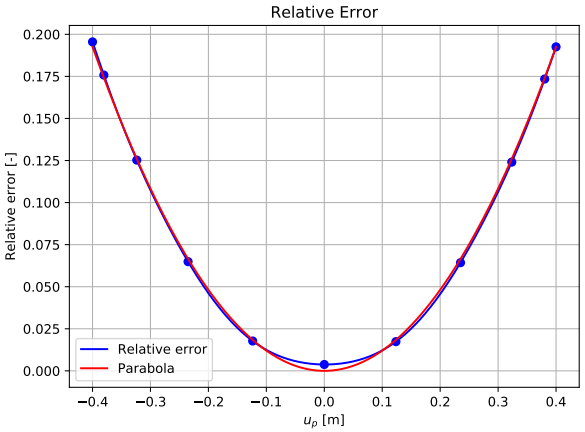

Figure 4. Relative error of Komperød (2018) compared to the calculations derived in the present paper. The figure also shows a parabola on the form $a\,u_p{}^2$, where a is a parameter set so that the parabola and the relative error graph match at $u_p = 0.4$.

terpretations.

Because the Lagrange multipliers are the sensitivities of the optimized value, in this case the minimum total potential energy, w.r.t. infinitesimal perturbations of the constraints, the Lagrange multipliers can easily be found from the approached derived in the present paper at the expense of additional iterations. That is, infinitesimal perturbations are added to the right hand side of Eq. 19 and the total potential energy is then re-optimized. The author has tested this method and found that it gives correct results. Further details and demonstrations of the method are beyond the scope of this paper.

8 Further Work

The work presented in this paper is the second milestone toward modeling subsea power cables and umbilicals during bending stiffess tests. The remaining milestones are (i) modeling nonlinear materials and (ii) modeling shear forces between the cable elements. The final model will be validated against the results from the physical bending stiffness tests. Once the model is completed and validated, it can be used for other calculations and simulations only by changing its loads and the boundary conditions.

This modeling work is part of Nexans Norway AS' continuous work on improving modeling and physical testing of subsea power cables and umbilicals. This work enables the company to install cables and umbilicals in ever deeper waters, in lower temperature areas, and under harsher weather conditions.

9 Conclusions

This paper improves the work of Komperød (2018) to correctly handle large deflections. Comparing the previous model and the improved model shows that the relative error of the previous model increases roughly by the deflection squared. For the example presented in this paper the largest relative difference is near 20%.

From the author's point of view, the only significant disadvantage of the improved model is that it depends on iterative optimization, while the previous model is solved explicitly. However, as shown in this paper, the analytical solution of the beam equation can be used as initial values for the iterative optimization. Using these initial values, both Newton's method and the BFGS method solve the optimization problem quickly, while the gradient decent method is very slow and may fail to converge to the correct values.

The author concludes that the modeling work presented in this paper is successful. This opens up for the next milestone, which is to include nonlinear materials in the model. The final goal of the overall R&D activity is to develop models which are feasible compromises between accuracy, complexity, and computation time, and which are validated against physical bending stiffness tests.

References

M. M. Dhaigude and K. I. Ekeberg. Validation of the loxodromic bending assumption using high-quality stress measurements - high tension case. In *Proceedings of the Twenty-sixth International Ocean and Polar Engineering Conference (ISOPE 2016), Rhodes, Greece*, 2016.

K. I. Ekeberg and M. M. Dhaigude. Validation of the loxodromic bending assumption using high-quality stress measurements. In *Proceedings of the Twenty-sixth International Ocean and Polar Engineering Conference (ISOPE 2016), Rhodes, Greece*, 2016.

L. Jordal, R. Slora, E. Vermeer, and M. Komperød. A novel bending stiffness rig for identification of subsea cables' and umbilicals' sensitivity to temperature under sinusoidal curvature oscillations. In *Proceedings of the Twenty-seventh International Ocean and Polar Engineering Conference (ISOPE 2017), San Francisco, California, USA*, 2017.

E. Kebadze. *Theoretical modelling of unbonded flexible pipe cross-sections*. PhD thesis, South Bank University, 2000.

M. Komperød. Deriving the beam equation using the minimum total potential energy principle and solving the equation numerically. In *Proceedings of the 59th International Conference of Scandinavian Simulation Society (SIMS 2018), Oslo, Norway*, 2018.

M. Komperød, J. I. Juvik, G. Evenset, R. Slora, and L. Jordal. Large-scale tests for identifying the nonlinear, temperature-sensitive, and frequency-sensitive bending stiffness of the NordLink cable. In *Proceedings of the 36th International Conference on Ocean, Offshore and Arctic Engineering (OMAE 2017), Trondheim, Norway*, 2017.

M. Lutchansky. Axial stress in armor wires of bent submarine cables. *Journal of Engineering Industry*, 91(3):687 – 693, 1969.

P. Maioli. Bending stiffness of submarine cables. In *Proceedings of the 9th International Conference on Insulated Power Cables (Jicable '15)*, 2015.

H. Reid. Massachusetts Institute of Technology - Lecture notes 18.330 Introduction to numerical analysis, 2014.

J. Tarnowski. Improved method of determining bending stiffness of underground cables. In *Proceedings of the 9th International Conference on Insulated Power Cables (Jicable '15)*, 2015.